Early TOTEM Running with the 90m Optics

The TOTEM Collaboration

Abstract

TOTEM proposes an optics with $\beta^* = 90\,\mathrm{m}$ for runs at the start of the LHC. It allows, at an early stage, to measure the total pp cross-section and the luminosity with a precision of about 5 % as well as the elastic pp scattering cross-section in the t-range from 0.04 to $1\,\mathrm{GeV}^2$. Furthermore, the horizontal beam position at the Roman Pot (220 m away from IP 5) and the horizontal vertex distribution in IP 5 can be determined at the micrometer level, helping the machine to calibrate their beam position monitors and to obtain a second measurement of the luminosity.

1 Introduction

For the luminosity independent total cross-section measurement TOTEM needs special high-β^* optics to reach the lowest possible values of the squared four-momentum transfer $-t$ in elastic pp scattering. Such a special optics with $\beta^* = 1540\,\mathrm{m}$ has been designed by the machine group for this purpose [1]. Since this optics will need a non-standard special injection scheme, its commissioning is complex and will only be foreseen at a later stage. We therefore propose an additional optics with a β^* of 90 m that uses the standard injection and the beam conditions typical for early LHC running: zero degree crossing angle and consequently at most 156 bunches together with low proton bunch densities ($\leq 5 \times 10^{10}$ p / bunch) resulting in a luminosity between 10^{28} and $6 \times 10^{29}\,\mathrm{cm}^{-2}\mathrm{s}^{-1}$. According to studies by the machine experts, this optics is much easier to commission than the final one.
In addition, the larger beam width of $\sigma_{y_{beam}} = 625\,\mu\mathrm{m}$ compared to $80\,\mu\mathrm{m}$ at $\beta^* = 1540\,\mathrm{m}$ facilitates the commissioning of the Roman Pot detectors and movements in the beginning of LHC operation.
This optics allows a measurement of the total cross-section and the luminosity with a precision of about 5 %. These early measurements are also essential for machine optimisation. The precise determination of the horizontal beam position at RP220 will calibrate the beam position monitors, and the horizontal vertex distribution at IP5 can be used for a second independent luminosity measurement based on machine parameters.

2 Properties of the Optics

The transverse displacement $(x(s), y(s))$ of a proton produced in an interaction at the IP with transverse coordinates (x^*, y^*), a momentum loss $\xi = \Delta p/p$ and a polar angle Θ^* can be generally expressed by the machine parameters [2], using the effective length L and the magnification v:

$$
\begin{aligned}
y(s) &= v_y(s) \cdot y^* + L_y(s) \cdot \Theta_y^* \\
x(s) &= v_x(s) \cdot x^* + L_x(s) \cdot \Theta_x^* + \xi \cdot D(s)
\end{aligned}
\tag{1}
$$

where

$$v(s) = \sqrt{\beta(s)/\beta^*} \, \cos \Delta\mu(s)$$
$$L(s) = \sqrt{\beta(s)\beta^*} \, \sin \Delta\mu(s)$$
$$\text{with the phase advance } \Delta\mu(s) = \int_0^s \frac{1}{\beta(s')} ds'$$

Figure 1 shows the optical functions along the beam line. To push the protons vertically into the acceptance of the forward detectors at the Roman Pot position of 220 m, the optics is optimised towards a large L_y and $v_y = 0$ (vertical parallel-to-point focussing for $\Delta\mu_y = \pi/2$) [3]. The emission-angle dependence of the horizontal displacement is eliminated by requiring a vanishing L_x ($\Delta\mu_x = \pi$).
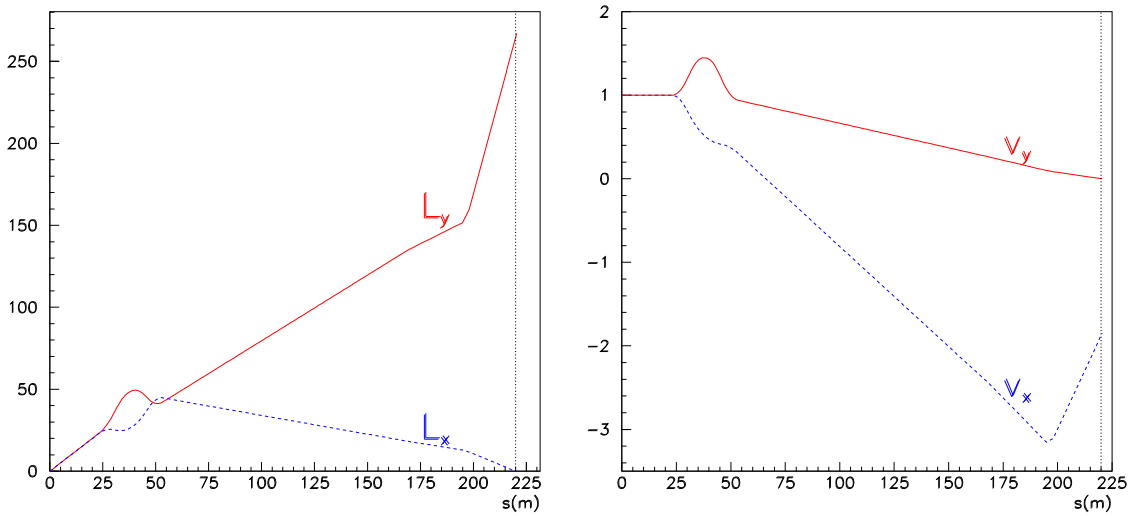

Figure 1: *Optical functions: left: effective lengths L_x, L_y [m]; right: magnification factors v_x, v_y.*

In case of elastically scattered protons detected at 220 m, Eqns. (1) can be rewritten as:

$$y(220) = L_y \cdot \Theta_y^*$$
$$x(220) = v_x(s) \cdot x^* \tag{2}$$

Figure 2 (left) shows the hit distribution for elastic-scattering events in the detectors at 220 m: the protons are detected in the vertical detectors, due to their transverse momentum: $t_y \equiv t \sin^2 \varphi \approx (p\,\Theta_y^*)^2$, where φ is the azimuthal production angle of the proton.

The distribution along the x-projection is mainly determined by the size of the interaction vertex (Figure 2, right): given the large statistics that can be accumulated within a few minutes of running, this allows an accurate determination of the horizontal beam position at the detectors location and the reconstruction of the horizontal beam profile at the interaction point at the micrometer level.
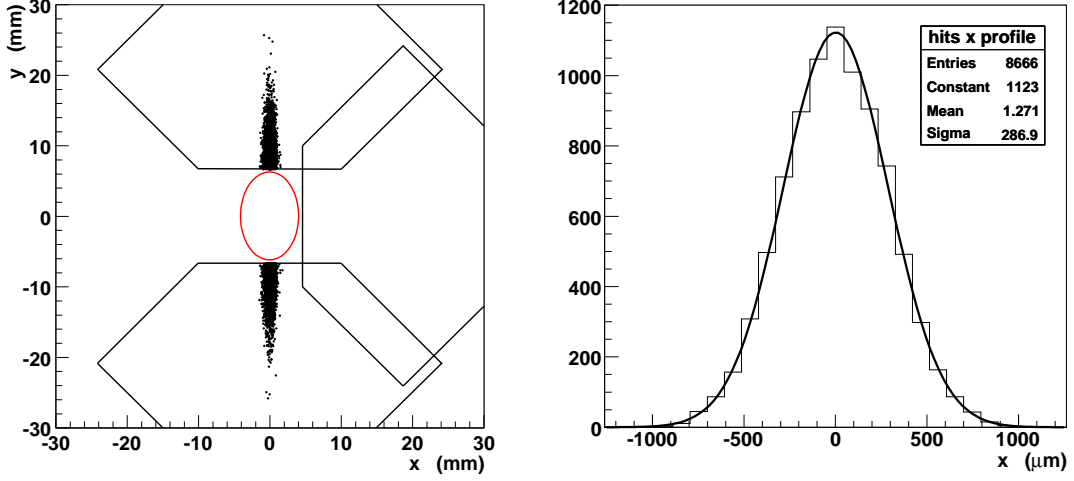
2

Figure 2: *Left: hit distribution for elastic-scattering events (generated according to the BSW model) in the detectors of RP220; the $10\,\sigma$ beam envelope is also shown. Right: hit distribution in the x-projection at RP220.*

3   Measurement of the Total Cross-Section

The total pp cross-section is related to the nuclear elastic forward scattering amplitude via the Optical Theorem which can be expressed as

$$\mathcal{L}\,\sigma_{tot}^2 = \frac{16\pi}{1+\rho^2} \left.\frac{dN_{el}}{dt}\right|_{t=0} \ . \tag{3}$$

With the additional relation

$$\mathcal{L}\,\sigma_{tot} = N_{el} + N_{inel} \tag{4}$$

one obtains a system of 2 equations which can be resolved for σ_{tot} or $\mathcal{L}$ independently of each other:

$$\sigma_{tot} = \frac{16\pi}{1+\rho^2}\frac{dN_{el}/dt|_{t=0}}{N_{el}+N_{inel}}\,, \tag{5}$$

$$\mathcal{L} = \frac{1+\rho^2}{16\pi}\frac{(N_{el}+N_{inel})^2}{dN_{el}/dt|_{t=0}} \tag{6}$$

Hence the quantities to be measured are:

- $dN_{el}/dt|_{t=0}$: the nuclear part of the elastic cross-section extrapolated to $t=0$;

- the total elastic rate N_{el}, related to the extrapolation $dN_{el}/dt|_{t=0}$;

- the inelastic rate N_{inel} consisting of diffractive ($\sim$18 mb at LHC) and minimum bias ($\sim$65 mb at LHC) events.

The parameter $\rho = \frac{\mathcal{R}[f_{el}(0)]}{\mathcal{I}[f_{el}(0)]}$, where $f_{el}(0)$ is the forward nuclear elastic amplitude, has to be taken from external theoretical predictions, e.g. [4]. Since $\rho \sim 0.14$ enters only in a $1+\rho^2$ term, its impact is small.

3

3.1 Inelastic Rate

The measurement of the inelastic rate is largely based on inclusive triggers with the trackers T1 and T2 and is hence almost independent of the machine optics, exceptions being Single Diffraction and Double Pomeron Exchange where leading protons are parts of the trigger signature. To reduce background from beam-gas events, a double-arm trigger strategy is preferred over single-arm triggering.

The estimate of the uncertainty – of mainly systematic nature from trigger losses – proceeds along the line explained in [2]. The result is 0.8 mb or 1 % of the predicted inelastic cross-section of 80 mb.

3.2 Elastic Rate and Cross-Section Extrapolation to t = 0

Elastic pp scattering events will be detected with the two RP stations placed symmetrically on both sides of the IP at ± 220 m.

The determination of total cross-section and luminosity according to Eqns. (5) and (6) requires two aspects of elastic scattering to be measured: the total elastic rate and the extrapolation of the differential cross-section $d\sigma/dt$ to the Optical point $t = 0$. Obviously, to be complete, the measured elastic rate has to be complemented by the extrapolated part, so that this extrapolation enters twice in the procedure.

In view of minimising the systematic error of the extrapolation, the elastic cross-section has to be measured down to the lowest reachable $|t|$-values (or $|t_y|$-values in the case of the $\beta^* = 90$ m optics). Under the usual assumption that the sensitive edge of the detector is at a distance of $10\,\sigma_{beam} + 0.5\,\text{mm} \sim 6.75\,\text{mm}$, from the beam center, protons with $|t_y| > 0.03\,\text{GeV}^2$ are observed in the 220 m detector, as shown in Figure 3.
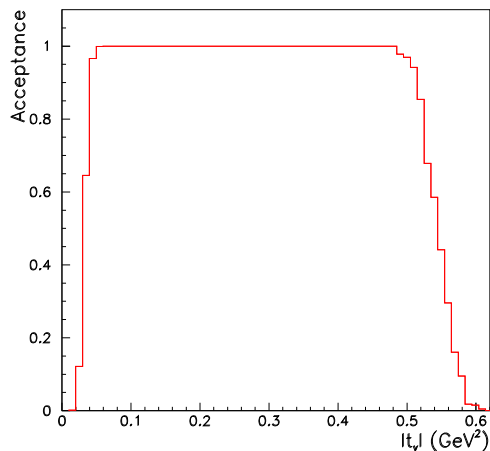

Figure 3: *Acceptance of the station RP220 in t_y.*

Most models [5] predict an exponential behaviour of the cross-secion up to $|t| \approx 0.25$ GeV^2, as shown in Figure 4. The deviations from a purely exponential shape are demonstrated by the exponential slope $B(t) = \frac{d}{dt} \ln \frac{d\sigma}{dt}$ in Figure 4 (right). One can conclude that for the models considered the deviations are small except for the model of Islam et al. In the t-range mentioned, the slope $B(t)$ can be well described by a parabola which is therefore used for the fitting function and the extrapolation. Since this quadratic behaviour of the slope characterises all the models, the extrapolation method is valid in a model-independent way.
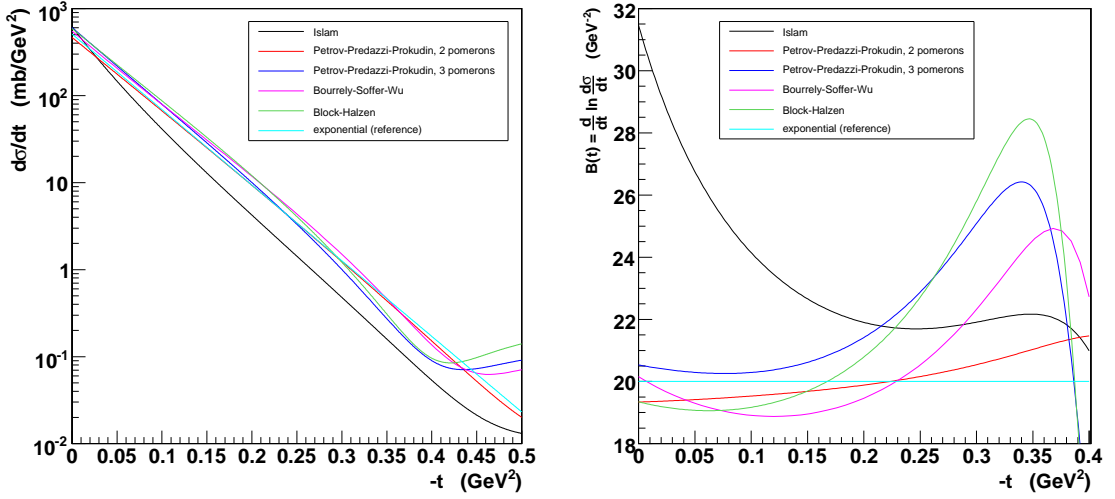
4

Figure 4: *Left: Differential cross-section of elastic scattering at 14 TeV as predicted by various models. Right: Exponential slope of the differential cross-section. The deviations from a constant slope show how the cross-sections differ from a pure exponential shape.*

With the $\beta^* = 90$ m optics, the acceptance starting point $|t|_{min} = 0.03\,\mathrm{GeV}^2$ lies well above the region where the delicate effects from the interference between nuclear and Coulomb scattering play a role. Hence no such perturbation needs to be included in the extrapolation procedure.

At the Roman Pot at 220 m the effective length $L_x(220\,\mathrm{m}) = 0$. Hence in this station only the y-component of the scattering angle is measured and only the t_y component reconstructed (Eqn. (2)). Using the azimuthal symmetry of the elastic scattering process and hence the equality of the distributions of t_y and t_x, the distribution $\mathrm{d}\sigma/\mathrm{d}t$ can be calculated from $\mathrm{d}\sigma/\mathrm{d}t_y$ distribution. Inversely, given the relation $t_y = t\sin^2\varphi$, one can convert the t distribution to the t_y distribution.
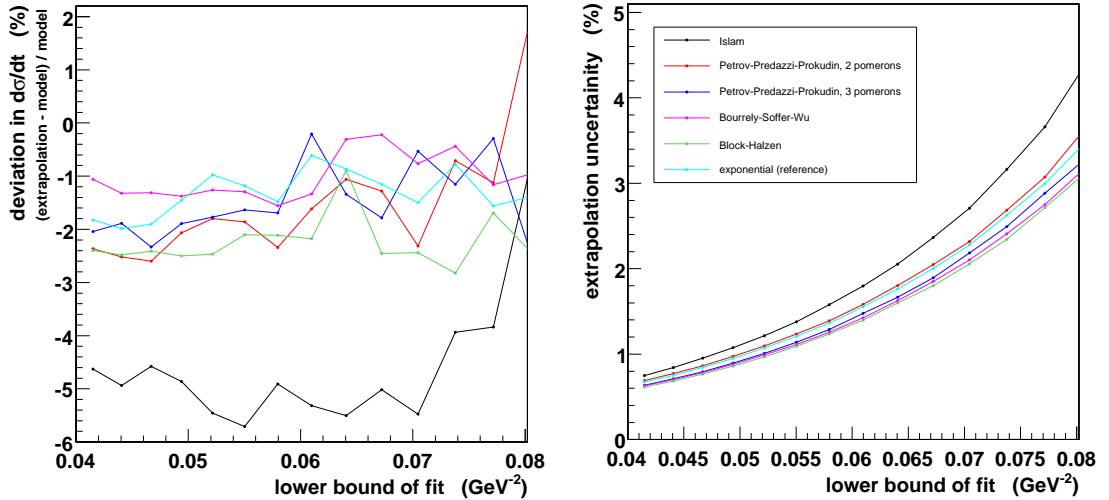

Figure 5: *Extrapolation results based on a MC simulation (not including the L_{eff} error) for an integrated luminosity of $2\,\mathrm{nb}^{-1}$ (about 5 hours of running at $10^{29}\,\mathrm{cm}^{-2}\,\mathrm{s}^{-1}$). The t_y distributions were fitted from the indicated lower bound to $0.25\,\mathrm{GeV}^2$. Extrapolated values were compared to those given by the hadronic models, and their relative deviation is shown in the left-hand plot. The corresponding statistical error is plotted in the right-hand figure.*

5

The simulated precision of the extrapolation is shown in Figure 5. The key contributions are the following:

- Smearing effects of the t-measurement which are dominated by the beam divergence ($\sigma_{beam} = 2.3 \ \mu$rad). Based on our preliminary MC simulations this contribution leads to a shift of $-2\,\%$ in the extrapolation result (Figure 5 left).

- The statistical error of the extrapolation for an integrated luminosity of 2 nb^{-1} corresponding to 2×10^4 s (about 5 hours) of running at a luminosity of 10^{29} cm^{-2} s^{-1} (Figure 5 right).

- Systematic uncertainty of the t-measurement: the dominant contribution comes from the uncertainty of the effective length L_{eff}. The expected precision of $2\,\%$ would lead to an extrapolation offset of about $3\,\%$ (not included in Figure 5, left).

  Due to the thick beam at $\beta^* = 90$ m ($\sigma_{y_{beam}} = 625\,\mu$m at RP220) compared to $\beta^* = 1540$ m ($\sigma_{y_{beam}} = 80\,\mu$m), and considering that $\frac{\Delta t}{t}|_{t=0} \propto \frac{\Delta_{detector}}{\sigma_{y_{beam}}}$, detector or beam position inaccuracies have a much smaller impact on the t measurement.

- Model-dependent deviations of the nuclear elastic pp cross-section from an exponential shape lead to a bias in the extrapolation (left-hand plot in Figure 5). Besides the Islam model which can be excluded or confirmed by the measured t-distribution at large t-values, the other models stay within $\pm 1\,\%$.

3.3 Combined Uncertainty

The total uncertainty of σ_{tot} in Eqn. (5) has the following contributions:

- Inelastic rate: $\frac{\delta(N_{inel})}{N_{inel}} \approx 1\,\%$ [1].

- Extrapolation of the elastic cross-section: $\frac{\delta(dN_{el}/dt|_{t=0})}{dN_{el}/dt|_{t=0}} \leq 4\,\%$.

- Elastic rate: $\frac{\delta(N_{el})}{N_{el}} \leq 2\,\%$. The high correlation between N_{el} and $\frac{\delta(dN_{el}/dt|_{t=0})}{dN_{el}/dt|_{t=0}}$ advantageously leads to a partial cancellation of errors. It is taken into account in the error combination below.

- The ρ parameter, estimated to be about 0.14 by extrapolating measurements at lower energies [4], enters σ_{tot} in the factor $\frac{1}{1+\rho^2} \sim 0.98$, and hence gives only a relative contribution of about $2\,\%$. Assuming a relative uncertainty of $50\,\%$ on ρ, determined by the error of the measurements at TEVATRON [6], we expect an uncertainty contribution of $\frac{\delta(1+\rho^2)}{1+\rho^2} = {}^{+2\,\%}_{-1.5\,\%} \approx 2\,\%$.

Combination of all these uncertainties by error propagation taking into account the correlations yields an error of $4\,\%$. With other, yet unknown, uncertainties at early running, we estimate the total uncertainty to be around $5\,\%$.

4 Measurement of Diffractive Events

Most diffractive processes (Single Diffraction SD and Double Pomeron Exchange DPE) have intact protons in the final state, characterised by their fractional momentum loss $\xi = \Delta p/p$, their squared four-momentum transfer t and their azimuthal production angle

---

[1] To avoid confusion with the cross-section, the notation for standard deviations is δ rather than σ in this document.
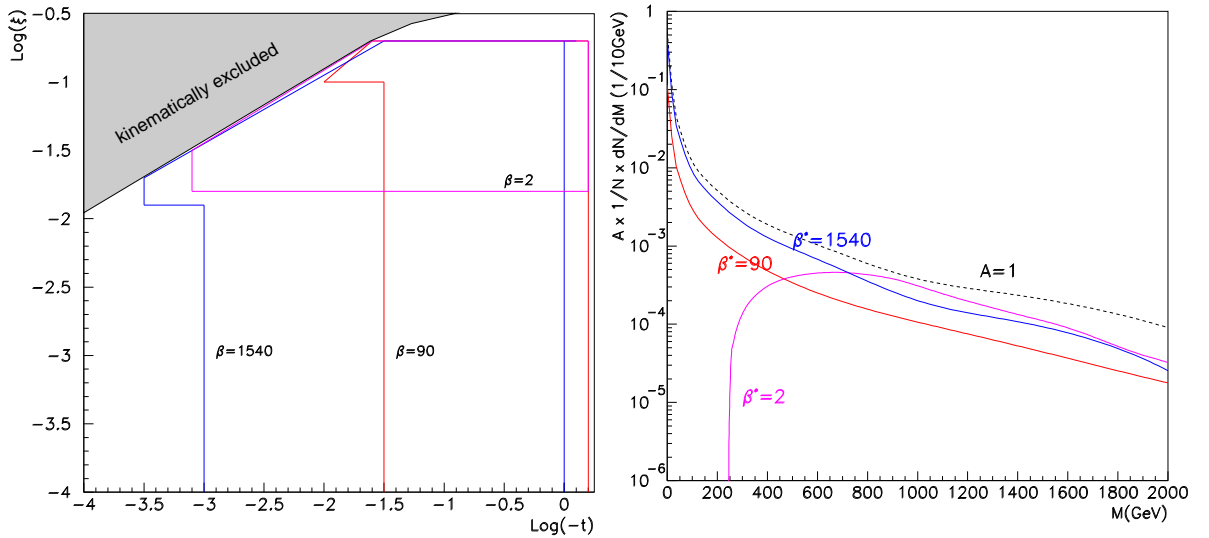
Figure 6: *Left: Acceptance in $\log_{10} t$ and $\log_{10} \xi$ for diffractive protons at RP220 for different optics. The contour lines represent the 10 % level. Right: Differential cross-section of DPE with (solid) and without (dashed) proton acceptance for different optics.*

φ. The acceptance of TOTEM's Roman Pot detectors for these leading protons depends considerably on the beam optics. Fig. 6 (left) shows the (t, ξ) acceptances integrated over φ for optics with $\beta^* = 0.5\,\mathrm{m}$ (2 m and 11 m are similar), 90 m and 1540 m. For $\beta^* = 0.5\,\mathrm{m}$, only protons with $\xi > 2\,\%$ are observed, corresponding to rather high diffractive masses ($M > 300\,\mathrm{GeV}$ in the case of DPE; see Fig. 6, right). For the two other optics, all ξ-values down to 10^{-8}, i.e. all diffractive masses, are accepted for $|t| > 3 \times 10^{-2}$ (2×10^{-3}) GeV^2 for $\beta^* = 90\,\mathrm{m}$ (1540 m). Consequently, a large fraction of the diffractive protons is observed: 65 % for $\beta^* = 90\,\mathrm{m}$ and 95 % for 1540 m, allowing first measurements of SD and DPE at LHC.

Owing to the vanishing effective length L_x at RP220 for the $\beta^* = 90\,\mathrm{m}$ optics, the dependence of the x-position on the emission angle Θ_x^* is eliminated, which leads to a ξ-resolution of 6×10^{-3}, mainly due to the vertex uncertainty. If the vertex is known from CMS with an accuracy of $30\,\mu\mathrm{m}$, the ξ-resolution improves to 1.6×10^{-3}.

5 Commissioning of the Optics

Statement from H. Burkhardt, AB-ABP:

The 90 m early TOTEM optics was studied in collaboration with the machine optics and commissioning working groups.

The LHC will be commissioned with the standard physics optics which has target physics tunes of $Q_x = 64.28$ and $Q_y = 59.31$ and a β^* of 11 m during injection and ramp in IR1 and IR5. For early physics operation, the crossing angle will be 0. The number of bunches will be limited (43 or 156), and the intensity per bunch will remain below 5×10^{10} protons. The β^* will be squeezed down in steps to $\beta^* = 2\,\mathrm{m}$ in IR1 and 5 to increase luminosity. Similarly, it should also be possible to un-squeeze β^* locally. Solutions with $\beta^* = 90\,\mathrm{m}$ in IR5 for early Totem operation have been studied. The un-squeeze results in a loss of phase advance and requires a small tune adjustment within the nominal tuning range of the LHC. As the 90 m option in IR5 is based on the standard optics and to the extent that it only requires the commissioning of the un-squeeze but no separate optics

7

for injection and ramp, we expect that the time needed for its commissioning will be significantly less than for the high beta (1540 m) optics. Commissioning of the $\beta^* = 90$ m optics is estimated to be of the same complexity as the commissioning of the early physics optics with $\beta^* = 2$ m, provided a small global tune change can either be accepted or easily corrected in early operation.

Acknowledgements

References

[1] A. Verdier: TOTEM Optics for LHC V6.5, LHC Project Note 369, 2005.

[2] TOTEM: Technical Design Report, CERN-LHCC-2004-002; addendum CERN-LHCC-2004-020.

[3] TOTEM collaboration: TOTEM Physics, Proceedings of 17th Rencontre de Blois: 11th International Conference on Elastic and Diffractive Scattering. Château de Blois, France, 2005. arXiv: hep-ex/0602025.

[4] J.R. Cudell et al., PRL **89**, (2002) 201801.

[5] M. M. Islam, R. J. Luddy and A. V. Prokudin: Near forward pp elastic scattering at LHC and nucleon structure, Int. J. Mod. Phys. A21 (2006) pp. 1–42.
Claude Bourrely, Jacques Soffer, and Tai Tsun Wu: Impact-picture phenomenology for pi+- p, K+- p and p p, anti-p p elastic scattering at high energies, Eur. Phys. J. C28 (2003), pp. 97–105.
V. A. Petrov, E. Predazzi and A. Prokudin: Coulomb interference in high-energy p p and anti-p p scattering, Eur. Phys. J. C28 (2003) pp. 525–533.
M. M. Block, E. M. Gregores, F. Halzen and G. Pancheri: Photon proton and photon photon scattering from nucleon nucleon forward amplitudes, Phys. Rev. D60 (1999) 054024.

[6] E710 Collaboration (N.A. Amos et al.), PRL **68**, (1992) 2433; E811 Collaboration (C. Avila et al.), Phys. Lett. **B 537**, (2002) 41.